International Journal of Pharmaceutics 505 (2016) 52–60

Contents lists available at ScienceDirect

International Journal of Pharmaceutics

journal homepage: www.elsevier.com/locate/ijpharm

Spatial distribution of oil depots monitored in human muscle using MRI

R.W. Kalicharan[a,b,*], P. Baron[c], C. Oussoren[b], L.W. Bartels[c], H. Vromans[a,b]

[a] Department of Clinical Pharmacy, Division of Laboratory & Pharmacy, University Medical Center Utrecht, P.O. Box 85500, 3508 GA Utrecht, The Netherlands
[b] Department of Pharmaceutics, UIPS, Utrecht University, P.O. Box 80082, 3508 TB Utrecht, The Netherlands
[c] Image Sciences Institute, University Medical Center Utrecht, The Netherlands

ARTICLE INFO

Article history:
Received 1 February 2016
Received in revised form 29 March 2016
Accepted 30 March 2016
Available online 31 March 2016

Chemical compounds studied in this article:
Benzyl alcohol (PubChem CID: 244)

Keywords:
Oil depots
Surface area
Spatial volume
MRI
Depot disappearance
Intramuscular
Release-rate

ABSTRACT

Oil depots are parenteral drug formulations meant for sustained release of lipophilic compounds. According to mass transport models, the drug-release rate from these injections is determined by the surface area of the oil depot. Until now, the size of the surface area of injected depots has not been assessed, however. MRI provides an excellent possibility to distinguish between water and adipose tissue. The aim of this study was to investigate whether MRI can be used to determine the shape and hence the surface area of oil depots in muscle tissue. The developed MRI-scan protocol is demonstrated to be suitable for visualising oil depots. It was applied to determine the surface area of 0.5 mL oil, i.m. injected in healthy volunteers. The mean (±RSD) surface area and volume of the depots recovered after injection was 755.4 mm^2 (±26.5) and 520.1 mm^3 (±24.6). It is shown that the depot disappearance from the injection site is very variable between volunteers. It is suggested that the oil is first solubilized and subsequently distributed. In all cases, the oil was not detectable after 14 days. These factors are relevant for the understanding of the mechanism by which compounds are released out of oil depots.

1. Introduction

Sustained delivery of drugs is an important method of drug administration for a number of diseases that require long-term drug treatment, such as psychiatric disorders (Covell et al., 2012; Novakovic et al., 2013; Uchida et al., 2013; Van Weringh et al., 1994) and hormone-dependent conditions (Edelstein and Basaria, 2010; Geusens, 1995; Morgentaler et al., 2008). The most commonly used drug-delivery systems, which can release drugs for a longer period of time, are parenteral injections. In general, long-acting parenteral injections are mostly administered by the intramuscular (i.m.) and subcutaneous (s.c.) route (Prettyman, 2005).

A considerable number of long-acting i.m. injections are available on the market. Conventional sustained release injections often consist of lipophilic compounds dissolved in vegetable oils. For example, arachis oil depots containing nandrolone decanoate (Bagchus et al., 2005; Minto et al., 1997; Wijnand et al., 1985) and castor oil depots containing testosterone undecanoate (Morgentaler et al., 2008) or estradiol valerate (Düsterberg and Nishino, 1982) have been marketed several decades ago and are still available on the market. Furthermore, i.m. oil depots are widely used as parenteral depot formulations of antipsychotic drugs, such as haloperidol decanoate (Van Weringh et al., 1994). Since these long-acting formulations are administered every few weeks, they require fewer injections and result in improved drug compliance.

Although many i.m. oil depots for sustained drug delivery have been marketed, the rate and extent of drug release is often difficult to predict. The drug-release and absorption rate from the oil solution is controlled by the drug partitioning between the oil vehicle and the tissue fluid (Kalicharan et al., 2016b). However, several other factors such as the injection site (Minto et al., 1997; Shaik et al., 2015; Soni et al., 1988), injection volume (Minto et al., 1997), the rate of bioconversion of the prodrug into the parent drug, the absorption and distribution of the oil vehicle and the extent of spreading of the depot at the injection site might affect the overall pharmacokinetic profile of the drug (Larsen et al., 2009; Weng Larsen and Larsen, 2009). Most studies focus on the

Abbreviations: TE, echo time; TR, repetition time; FOV, field of view.

* Corresponding author at: Department of Clinical Pharmacy, Division of Laboratory & Pharmacy, University Medical Center Utrecht, P.O. Box 85500, 3508 GA Utrecht, The Netherlands.
E-mail address: r.kalicharan@umcutrecht.nl (R.W. Kalicharan).

http://dx.doi.org/10.1016/j.ijpharm.2016.03.064
0378-5173/

pharmacokinetics of the drug rather than on the fate of the oil depot formulation (Bagchus et al., 2005; Luo et al., 1997; Morgentaler et al., 2008; Soni et al., 1988; Van Weringh et al., 1994; Wijnand et al., 1985). Thus far, only few researchers have reported on the rate and extent of disappearance of the injected formulation. In 2001 Larsen et al. reported a disappearance half-life of 21.4 days of an iodine-125 labelled oil depot after i.m. injection in the lower back of pigs (Larsen et al., 2001). Radioactivity was monitored by placing the scintillator probe directly on the skin surface. To date, no studies on the fate of oil depots in humans have been published yet.

Drug-release rate from depot injections are estimated according to mass transport models. A parameter for this release rate is the surface area of the oil depot (Nelson and Shah, 1975). These mass transport models are often based on the assumption that the injected depots are spherically shaped. However, until now, the shape, and therefore the associated surface area, of injected depots had not been known. The surface area is the interface between a hydrophilic and lipophilic phase. In the case of an i.m. oil depot, the interface is formed by the muscle interstitial fluid and the oil formulation, respectively. Since the size of the surface area of the oil depot determines the extent of mass transport over the interface, this plays an important role in the rate and extent of drug release from i.m. injected oil depots (Nelson and Shah, 1975).

Until now, there are no published methods to visualise small volumes of oil in situ without an invasive procedure. Hence, the value of the surface area of a perfect sphere is used for modelling the release rate of substances. As a result, absorption profiles of active substances originating from oil depots cannot be accurately predicted and the pharmacokinetic profiles and therapeutic efficacy cannot be estimated.

In this study, magnetic resonance imaging (MRI) was used to determine the surface area of oil depots in a non-invasive manner. MRI provides excellent soft tissue contrasts and this feature can also be used to distinguish water and adipose (fat) tissue. The fat/water contrast in images can be provoked in two different ways: (1) by signal weighting on the basis of the magnetic relaxation times (T1 and T2 for the longitudinal and transverse magnetization component, respectively) of protons in the oil depot and of those in the surrounding tissue or (2) by the difference in chemical shift (Philips Medical Systems, 2008). Each nuclei has a different spin frequency and this frequency is also influenced by nearby nuclei (e.g. in a molecular environment by chemical bonding). Chemical shifts are relative frequency differences within one voxel. Initially, both imaging techniques were used in preliminary studies. Later on, the focus was shifted to the difference in chemical shift, because this technique is generally known for obtaining fat fractions (small portions of lipophilic liquid or tissue) adequately in a quantitative result. This is relevant in this current study.

The aim of this study was to investigate whether MRI can be used to determine the surface area of oil depots in muscle tissue in situ. Subsequently, the developed MRI-scan protocol was applied to determine the surface area of i.m. injected oil depots in human volunteers.

2. Material and methods

2.1. Materials

Fresh pigskin (from epidermis till muscle tissue) was obtained from the Central Laboratory Animal Research Facility (Utrecht University, the Netherlands). Fresh chicken breast (muscle tissue) was obtained from the local butchery. Sesame oil (Ph. Eur.) and benzyl alcohol (Ph. Eur.) were purchased from Fagron BV (Capelle aan den IJssel, the Netherlands). A BD Microlance 3®, 21-gauge needle was used in all experiments.

2.2. Oil depot injections

Oil depots contained sesame oil mixed with 10% (m/v) benzyl alcohol, unless otherwise defined. Subsequently, the mixture was sterilised by filtration (0.2 μm, Mini Kleenpak Fluorodyne II, Pall Corporation, USA) and packed under current Good Manufacturing Practice conditions in the Clinical Pharmacy University Medical Center Utrecht, the Netherlands.

2.3. Preliminary studies

2.3.1. Magnetic resonance imaging and set-up

Preliminary MRI scans were performed on a clinical 3.0-T MRI-scanner (Achieva, Philips Healthcare, Best, the Netherlands). T1 and T2 relaxation times of the oil depot injections and tissues were determined with the following parameters: “mixed weighted 2D sequence”- sequence (echo time (TE) = 20, 40, 60 and 80 ms; repetition time (TR) = 700 and 2000 ms; field of view (FOV) = 70 × 150 × 150 mm; slice thickness = 1 mm). MR Spectra were obtained with the following parameters: “single voxel press”-sequence (TE = 31 ms; TR = 2000 ms; FOV = 10 × 10 × 10 mm; number of scans = 128).

Examined liquids were 100% sesame oil and sesame oil mixed with 10% (m/v) benzyl alcohol that were packed in plastic syringes. Syringes were fixed to pig tissue with tape and placed in a 2 L water bath (36.4 °C). The whole set-up was placed in centre of the bore of the 3.0-T MRI-scanner and a micro coil (inner diameter 47 mm), the detection device, was used as a radio frequency (RF)-receive coil.

2.4. Oil in muscle tissue studies

2.4.1. Magnetic resonance imaging

Both *ex vivo* animal and *in vivo* human imaging studies were performed on a clinical 1.5-T MRI-scanner (Achieva, Philips Healthcare, Best, the Netherlands). The parameters for the MRI-scan protocol were: “multi-echo 3D spoiled gradient-echo”-sequence (also known as the Dixon-scan), voxel size = 1 × 1 × 1 mm, TE0 = 2.1 ms, ΔTE = 1.6 ms, repetition time = 25 ms, flip angle = 50°). Field of View: 180 × 164 × 80; total scan duration = 4 min and 4 s. A SENSE Flex S coil, the detection device, was used as a RF-receive coil.

2.4.2. Sensitivity

Sensitivity was determined by a visual observation of the oil liquid in muscle tissue after MRI scan. For this, chicken breast tissue was injected with 0.05 mL sesame oil mixed with 10% (m/v) benzyl alcohol. Subsequently, this tissue was placed in centre of the bore of the MRI scanner. Three scans were conducted to assess the visibility of oil liquid in muscle tissue.

2.4.3. Accuracy and precision

Intra-and inter-scan accuracy and precision of spatial oil volume determination were performed with a fixed volume of oil. A commercial soft gel capsule (alfacalcidol 0.25 μg, Pharmachemie B.V., Haarlem, the Netherlands) containing arachis oil was inserted into chicken breast. The real capsule volume was determined in water: the increased water volume represents the capsule volume after the capsule was immersed in water. This experiment was repeated three times, with different capsules.

Initially, the tissue was scanned with MRI for the intra-scan accuracy and precision (n = 3). Subsequently, inter-scan accuracy and precision were conducted by repositioning the surface coil slightly: after the first scan (*Position 1*), the surface coil was repositioned (*Position 2*) and the tissue was scanned again (n = 3). Accuracy was determined by comparing the mean real capsule volume with the volume obtained from post processing and the

obtained volumes between Position 1 and 2. A volume difference of ±3% was considered as acceptable. The precision (relative standard deviation; RSD) was calculated by dividing the standard deviation (SD) by the square root of N. A RSD of <10% was considered as acceptable.

2.4.4. Subjects

Four male volunteers participated in the study (characteristics of the volunteers are summarized in Table 1). Ethical approval for the study was obtained from the ethical committee of the University Medical Center Utrecht, the Netherlands (protocol number: 14-401/D). Written informed consent according to the latest Declaration of Helsinki was obtained from all volunteers. Inclusion criteria were: healthy males with an age between 18 and 65 years old. Exclusion criteria: claustrophobic, metal clips or wires in the upper arm, implanted peacemakers, allergies to sesame oil or benzyl alcohol, other depots present in the same muscle or smoking.

2.4.5. Clinical study

Before injection, a planning (blank) scan was made by positioning the surface coil on the upper arm of the volunteer. Immediately after the planning scan, an oil depot with a volume of 0.5 mL was injected in the left biceps brachii (upper arm). The volunteers remained on the MRI table and were not allowed to move the upper arm during the planning scan, the injection and the scan immediately after the injection. Initially, MRI scans of the injection site were made in week 2, 3 and 4 after injection, unless otherwise stated.

2.5. Volume and surface analysis

Firstly, the volume and surface area of the oil depot were determined by obtaining fat fractions maps directly after the MRI scan. These fat fraction maps were calculated using the clinical software program of Philips Healthcare and exported as PAR/REC-files. Data processing was performed using MeVisLab 2.7 (MeVis Medical Solutions AG, Bremen, Germany) (Ritter et al., 2011).

Secondly, the fat fraction images were used to visually delineate the oil depot from the muscle tissue, using an isoline spline drawing technique as implemented in an in-house developed program based on MeVisLab (Kuijf, 2013; Ritter et al., 2011). This manual delineation was used because it was unknown whether volunteer movement or the presence of BOH in the oil depot had any influence in obtaining the oil volume automatically. Otherwise, automatic volume and surface calculations from the fat fraction maps were preferred.

Lastly, after delineation, a binary image (1 = 100% fat and 0 = 100% water) was obtained and interpolated and combined with the triangulation method (with cut-off voxel intensity value of 0.5). This was used to create a smooth surface area from which the volume and surface area could be determined. The triangulation method was performed using the IsoSurface module, included in MeVisLab 2.7 (Ritter et al., 2011). No analysis was performed in the absence of a visual oil depot.

Table 1
Volunteer baseline characteristics (n = 4).

	Mean ± SD
Age (years)	37.8 ± 12.8
Length (meters)	1.8 ± 0.1
Weight (kilograms)	79.8 ± 12.6
BMI (kg/m^2)	23.5 ± 2.9

3. Results and discussion

This study reports the development of a MRI method to visualise the surface area of an i.m. oil depot injection. Firstly, preliminary studies were conducted in order to develop an appropriate MRI-scan protocol. Secondly, the developed scan protocol was assessed on suitability for use in humans. Lastly, the MRI-scan protocol was used to determine the surface area of i.m. injected oil depots in healthy volunteers.

3.1. Development and suitability of the MRI-scan protocol

3.1.1. Preliminary studies

Distinction between the oil depot and muscle tissue was firstly attempted based on signal weighting: differences in T1 relaxation times may cause an adequate fat/water contrast image. These differences were obtained in successive layers of the scanned body area, which result in a tomographic map. A tomographic map is a matrix of successive, two-dimensional images (pixels) to form volumetric pixels (voxels). The preliminary studies were conducted *ex vivo*. To represent the human arm tissue, pigskin was used consisting of muscle and subcutaneous tissue. Syringes with oil depot liquid were externally attached to pig tissue. This research showed a significant difference in relaxation times between oil (with or without benzyl alcohol) and muscle tissue (Table 2). The relaxation times of adipose tissue are reported in Table 2.

Despite the fact that significant differences in relaxation times between oil (with or without benzyl alcohol) and muscle tissue was seen, this fat/water contrast image based on signal weighting was not further developed. The decision was taken, because the relaxation times of adipose tissue and oil were relatively similar (within 10% of each other). Before the start of the clinical study, it was not clear how deep the oil depot would be injected into the biceps brachii. A confusion between adipose tissue and oil depot was possible.

Contrast images were therefore created using the differences in chemical shift. This technique is generally known as a more reliable method for quantitative spatial volume determination. It gives fat fractions as output data variable, which was used for oil depot volume calculations. The development started by obtaining MR spectra of pure sesame oil and sesame oil + 10% benzyl alcohol (BOH) (Fig. 1). Unfortunately, the MR spectra corresponded to the MR spectrum of adipose tissue (Querleux et al., 2002; Ren et al., 2008), which also contains triglycerides (Ren et al., 2008). Therefore, automatic contrast imaging to obtain the oil depot could not be done. Fig. 1 shows a benzyl alcohol peak in the sesame oil + 10% benzyl alcohol sample around 6 ppm. By focussing on this peak, contrast images could be created. Unfortunately, oil depots are fully depleted of benzyl alcohol after three days (Kalicharan et al., 2016a), so this peak will not appear anymore after three days. The here developed visualisation method must be applicable to visualise the oil depot directly after injection, during the release of benzyl alcohol and after benzyl alcohol depletion.

Table 2
Relaxation times of pig tissue and sesame oil (pure or mixed with benzyl alcohol (BOH)) are presented as mean ± standard deviation (n = 3). Temperature = 36.4 °C. BOH = benzyl alcohol.

	Relaxation time (ms)	
	T1	T2
Muscle tissue	1475.0 (305.7)	3.8 (1.6)
Adipose tissue	336.3 (16.0)	50.7 (0.8)
Sesame oil	354.7 (3.9)	53.1 (0.5)
Sesame oil + 10% BOH	322.3 (5.5)	48.6 (0.4)

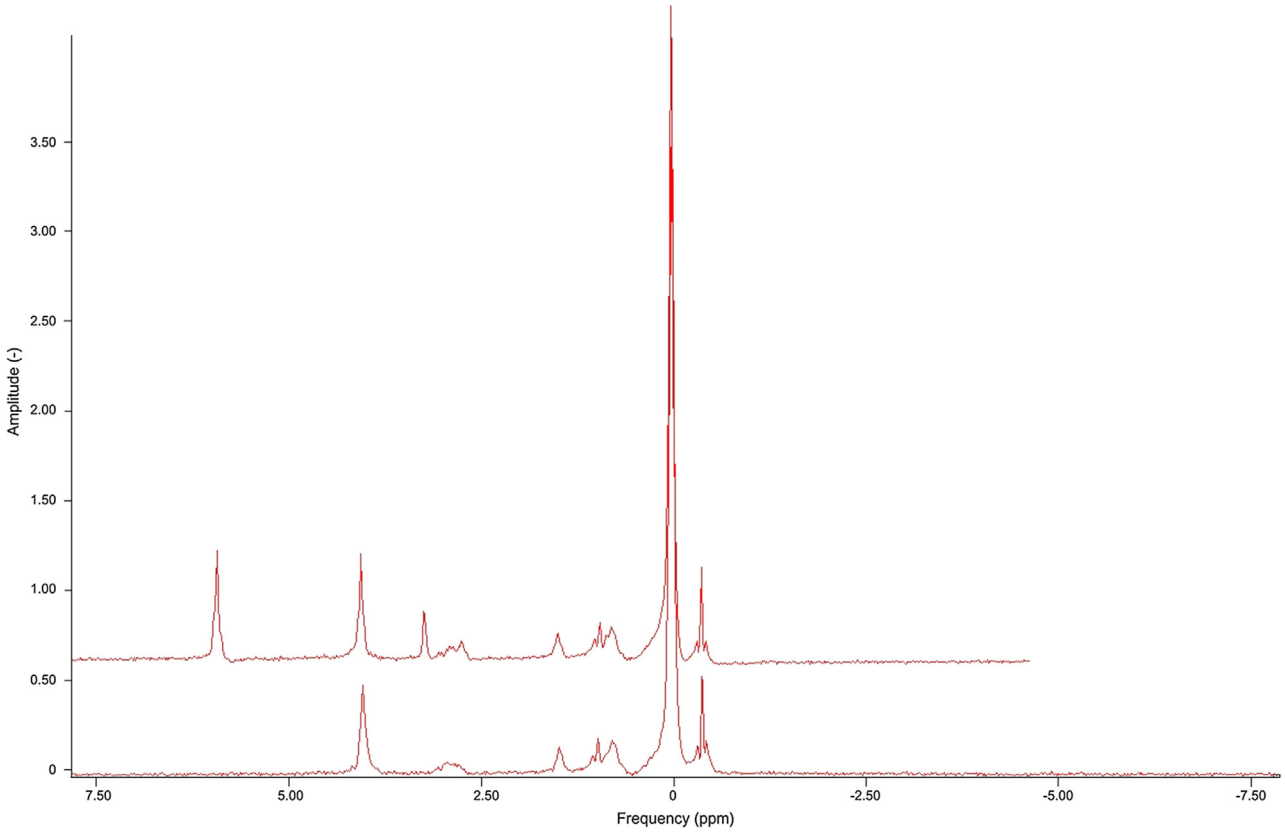

Fig. 1. MR spectra images of pure sesame oil (lower red line) and sesame oil mixed with 10% benzyl alcohol (upper red line). Specific benzyl alcohol in sesame oil frequency was around 6 ppm. (For interpretation of the references to colour in this figure legend, the reader is referred to the web version of this article.)

As mentioned before, fat/water contrast images were created using the differences in chemical shift. A commonly used method is the Dixon method (Dixon, 1984), which is an existing MRI-scan method to discriminate between fat and water fractions (Hu et al., 2010; Ma, 2008). This method was then modified to visualise the oil depot from muscle tissue more adequately, even on a lower magnetic field strength MRI-scanner. As a result, it was decided to continue the *ex vivo* experiments and *in vivo* study with a clinical 1.5-T MRI-scanner

The surface area and volume of the oil depot were determined from the raw data of the complete tomographic map. The fat fraction is measured in voxel intensity value, wherein a voxel intensity value of zero means that a voxel contains 100% water and a voxel intensity of 1 is labelled as 100% oil. In this study, the voxel intensity value of 0.5 was arbitrarily chosen as a cut-off value for a fat fraction per voxel. The oil volume was obtained by the summation of all fat fractions. All square surfaces (1 mm^2) at the interface between oil and water formed the total surface area of the depot. Via post-processing, three-dimensional images were built up from voxels.

3.1.2. Sensibility, accuracy and precision

Sensibility, accuracy and precision studies of this method were investigated on samples of chicken breast muscle instead of pig tissue, because of the lower amount of fat in chicken tissue.

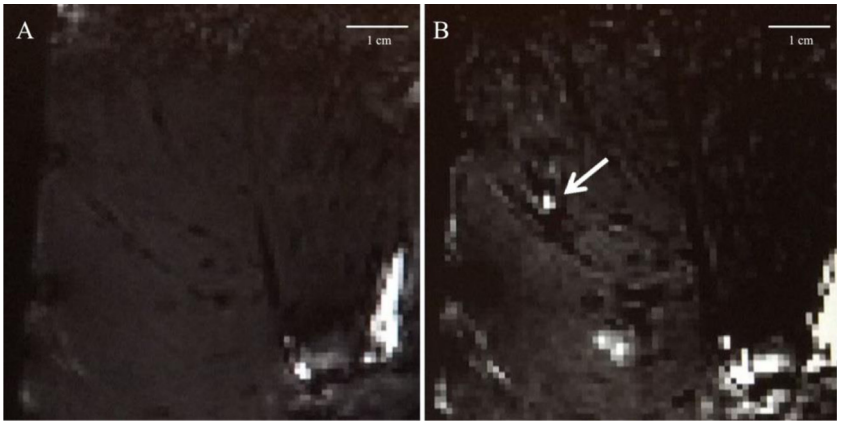

Fig. 2. Chicken breast muscle was used for this experiment to determine the sensitivity of the scan procedure. Blank sample (a) was injected with 0.05 mL sesame oil mixed with benzyl alcohol (10% (m/v)) (b). The white arrow indicates the oil liquid.

In Fig. 2, the result of a MRI scan to determine the sensitivity is shown. Blank sample of 0.05 mL sesame oil mixed with benzyl alcohol was injected in chicken breast muscle. The mixture is harder to distinguish from muscle tissue because of a smaller difference in relaxation times compared to pure sesame oil (Table 2). Immediately after injection, muscle tissue was scanned with the here developed scan protocol. The scan was visually examined by voxel intensity value, based on white pixels. The number of white pixels is a measure for the fat fraction in muscle tissue.

Scan of muscle tissue with sesame oil mixed with benzyl alcohol (0.05 mL) is shown in Fig. 2B. The oil depot resulted in 3 pixels and 8 voxels. Thus, the developed method was sensitive enough to determine 0.05 mL 10% (m/v) benzyl alcohol in sesame oil.

Accuracy and precision of the scan protocol were performed with a fixed oil volume, which represented the oil depot. The fixed volume was an oil capsule, containing arachis oil and was inserted into fresh chicken breast. As with the sensitivity determination, voxels were obtained for accuracy and precision determination.

The oil capsule had a mean (±RSD) volume of 240 mm^3 (±20) (n = 3). The results of volume determination with MRI are summarized in Table 3. Normally, MRI-signals from objects of interest are received via surface coils. This is a coil made of copper and receives spin frequencies from protons. This experiment was repeated with a slightly changed position of the surface coil to determine the volume repeatedly. Obtained volumes of position 1 and 2 after post-processing were 244.6 (±5.4) and 240.6 mm^3 (±1.3), respectively. This was comparable with the real capsule volume. Regardless to the position of the surface coil, the obtained volume was not significantly changed and met the predefined requirement of ±3% in volume difference. The attachment of the surface coil to enrolled volunteers is therefore not very critical. Repeated analysis resulted in a precision of maximal 5.4%, which met the predefined requirement of <10%.

In addition, a reconstruction of the capsule was made by post-processing (Fig. 3). It appeared that the surface of the capsule was not perfectly spherical. An explanation for these irregular edges could be that the shell of the soft capsule consists of gelatine. Gelatine is composed from animal material, which may contain fat.

The suitability experiments showed that this newly developed MRI-scan protocol was sensitive enough to determine small amounts of oil depots. Furthermore, the obtained oil volume was recovered accurately and precisely during post-processing. Subsequently, the developed MRI-scan protocol above was used in a clinical study with healthy volunteers.

Table 3
Volume and surface area of oil capsule determined by post processing.

	Volume (mm^3)		Surface area (mm^2)	
Position	1	2	1	2
N	3	3	3	3
Mean	244.6	240.6	199.7	209.8
RSD (%)	5.4	1.3	2.2	3.2

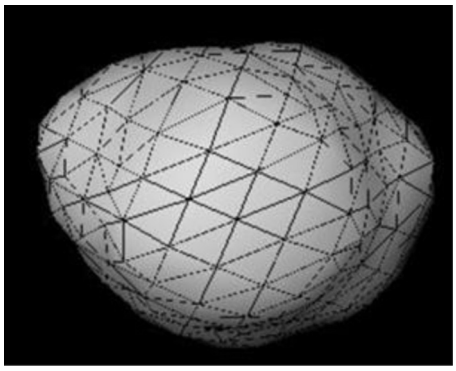

Fig. 3. Reconstructed alfacalcidol capsule. The edges were irregular instead of a smooth, round capsule surface.

3.2. Clinical study

To study the surface shape of an oil depot in human, four healthy male volunteers were injected with an oil depot in the biceps brachii of the left arm. The baseline characteristics of the volunteers are summarized in Table 1. The study was designed to scan each volunteer four times in total. This number was requested to keep the burden for the volunteer as low as possible, while we

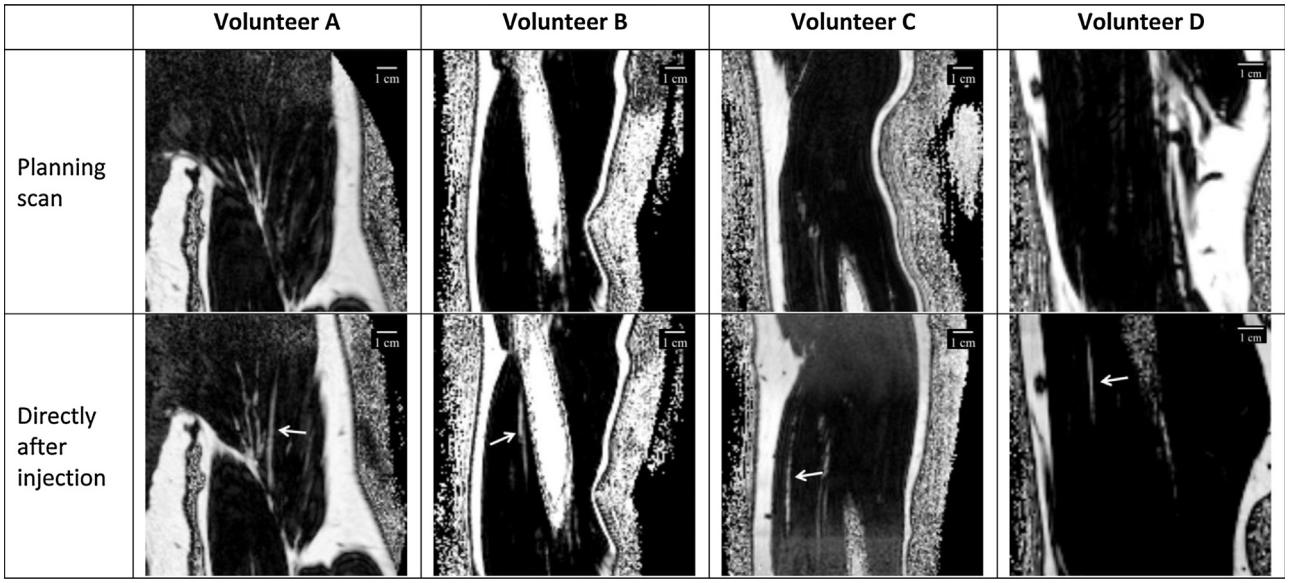

Fig. 4. An overview of the upper arms of the volunteers. Top row shows the planning (blank) scan where a proper injection site was chosen. The second row showed the oil depot directly after injection (white arrow). The white tissues represent tissues that contain a higher fat/water ratio: subcutaneous and bot tissue. Dark areas contain relative more water, such as muscle tissue.

were still able to obtain the rate of disappearance from the injection site (zero- or first-order clearance kinetics).

The mean (±RSD) surface area and volume of the depots recovered after injection was 755.4 mm^2 (±26.5) and 520.1 mm^3 (±24.6). All oil depots were injected between 15 and 22 mm deep. No adverse reactions upon injection were reported.

As can be seen in Fig. 4, the injected depots were oblong in all volunteers. This stretched shape was confirmed by post-processing the data (Fig. 5). Apparently, the oil liquid follows the fibres in muscle. A schematic cross-section of the muscle before and after injection is represented in Fig. 6. The resolution of the MRI scanner was not sufficient enough to visualise perimysia and fascicles. Therefore, it cannot be determined how the oil liquid is spread through the perimysium and several fascicles. However, based on the size of the needle, it is assumed that the perimysium between fascicles will be pierced by the injection needle. Consequently, as a result of the injection, the oil liquid will spread across multiple fascicles and will form a bulk (continuous) phase (Fig. 6). This is substantiated by the visualisation of the oil depots immediately after injection (Fig. 5), wherein the oil depot forms a thin, long shape.

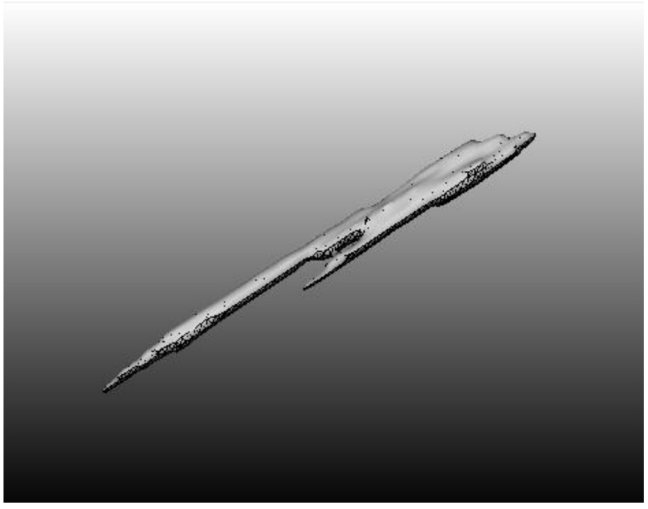

Fig. 5. The oil depot directly after injection from volunteer C was obtained via post-processing whereby every voxel was analysed to the amount of voxel intensity. This 3D-picture contains every voxel that had an voxel intensity of ≥0.5, which was marked as fat-fraction.

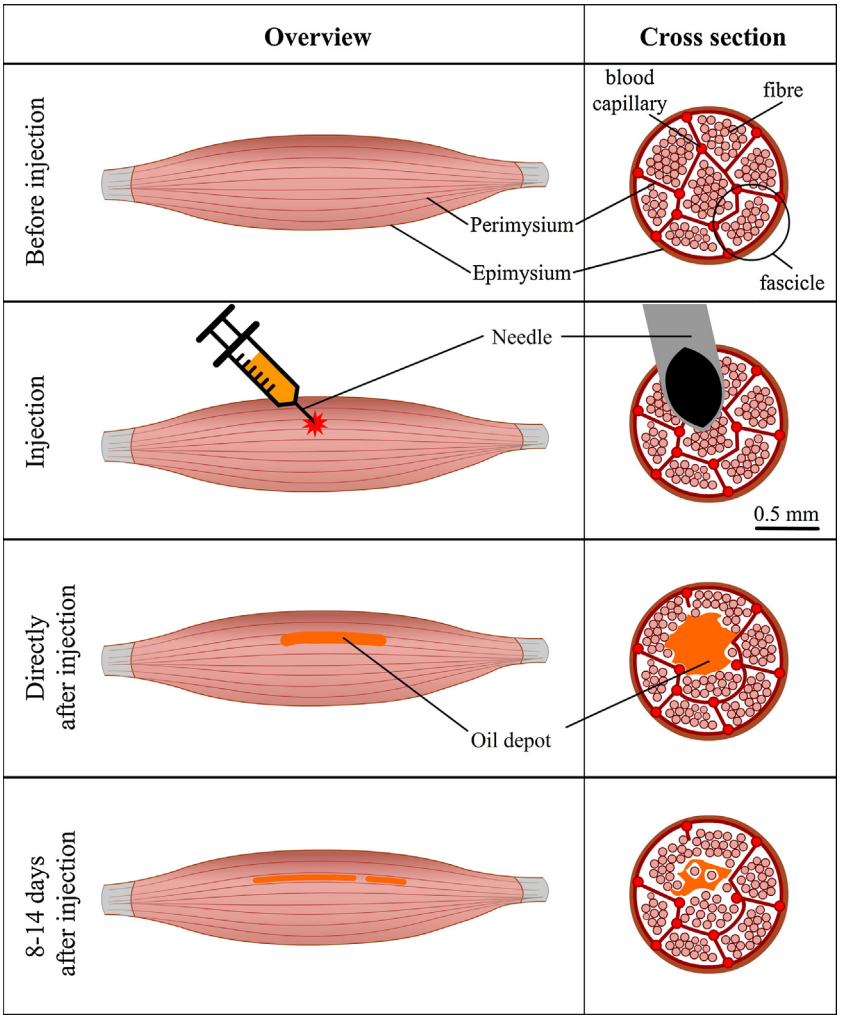

Fig. 6. A schematic image of the muscle before and after injection. The diameter of the needle is 0.5 mm. It is assumed that the perimysium between fascicles is pierced by the injection needle. Consequently, as a result of the injection, the oil depot will spread across multiple fascicles and push aside the muscle fibres to form a bulk (continuous) phase.

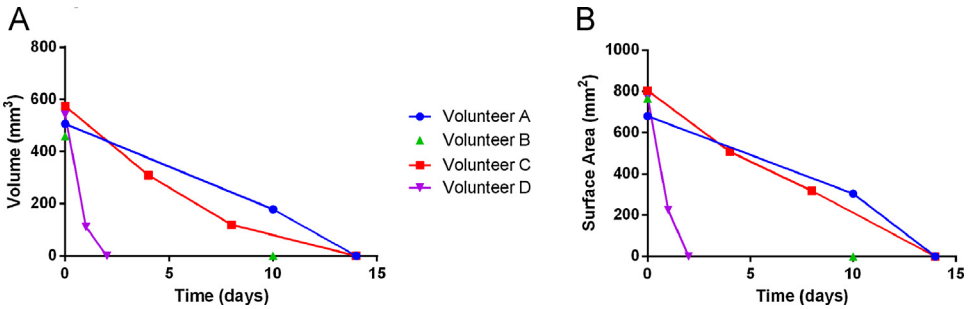

Fig. 7. The depot volume (A) and surface area (B) reduced in time after injection. No line was drawn for volunteer B, because it was unclear at which time-point the depot disappeared.

3.2.1. Disappearance rate from the injection site

In addition to visualisation of the shape of the oil depot, the rate of disappearance of the oil depot from the injection site was also determined. As stated before, the reported disappearance half-life of an i.m. depot in pigs was 21.4 days (Larsen et al., 2001). Based on these data, it was estimated that the depot would stay for 4–5 weeks at the injection site. Therefore, a total of 4 MRI-scans were scheduled for every volunteer in the consecutive weeks after injection.

Volunteer A and B received the first oil injections and scanned according to the scan schedule as mentioned in the study protocol. In the second week after injection, the oil depot volume in volunteer A decreased from 506.0 to 178.6 mm^3; this was a reduction of 327.4 mm^3 (−65%) within 8 days (Fig. 7A). Furthermore, the depot could not be visualised anymore at day 14. Speculatively, a merge with adipose tissue occurred or the oil depot was fully stretched out, probably due to oil digestion. See an evaluation of applied method below.

The second MRI-scan for volunteer B was, as scheduled, in the second week after injection. The depot was not visible anymore at that moment (Fig. 7). Hence, it was unclear when the depot disappeared exactly, but it was within 2 weeks.

The scan schedule for volunteer C and D was therefore intervened. The period between the MRI-scans for volunteers C and D was shortened. The oil depot in volunteer C was determined at day 0, 4, 8 and 14 (Fig. 7). Clearly, the oil depot was split into 2 or more parts (Fig. 8).

The oil depot in volunteer C still showed a fast disappearance rate from the injection site (Fig. 7). Therefore, it was decided to modify the scan intervals for volunteer D by scanning the upper arm every day with a maximum of 4 scans. The depot volume was 540.8 mm^3 immediately after injection. The volume was reduced by 430 mm^3 after the first day. A full disappearance was seen at day 2. This volunteer had normal motility during these days. There was neither sport activity, nor heavy objects were lifted.

3.3. Evaluation of applied developed method in current clinical study

The here developed MRI scan method is accurate, precise and sensitive and it is therefore applied in the current clinical study. An arbitrary cut-off voxel intensity value of 0.5 was used to label fat fractions. Fig. 9 shows two other evaluated cut-off voxel intensity values. Logically, the surface area and volume increases by a cut-off voxel intensity value of 0.3 for the fat fraction, whereas these oil depot properties decrease when using 0.7. Interestingly, the 3D image shows a smaller oil depot by a cut-off voxel value of 0.7. It seemed that the whole oil depot contained less fat fractions by, speculatively, an increased amount of water per voxel. This may

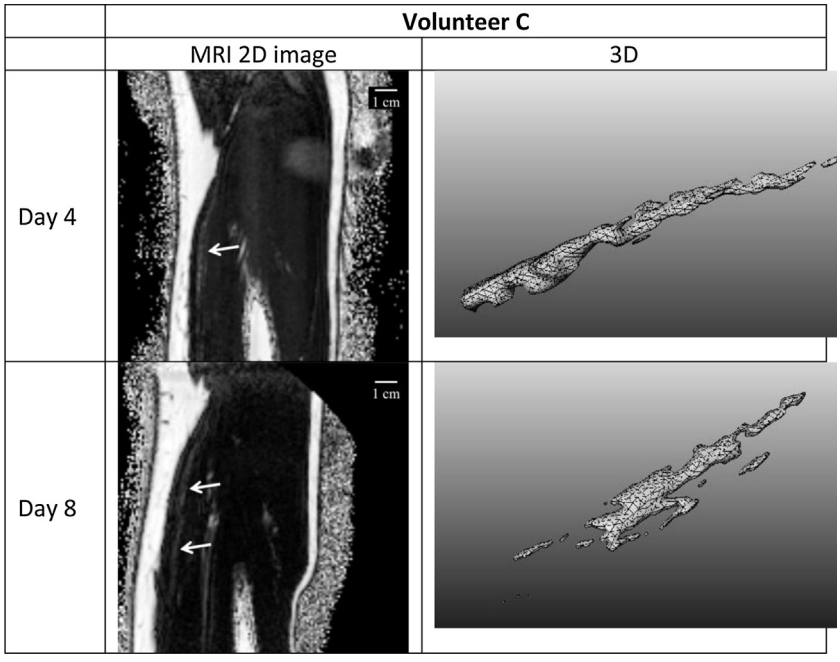

Fig. 8. Visualisation of the oil depot in volunteer C. The images show the depot at day 4 and 8. White arrows indicate the oil depot in tissue.

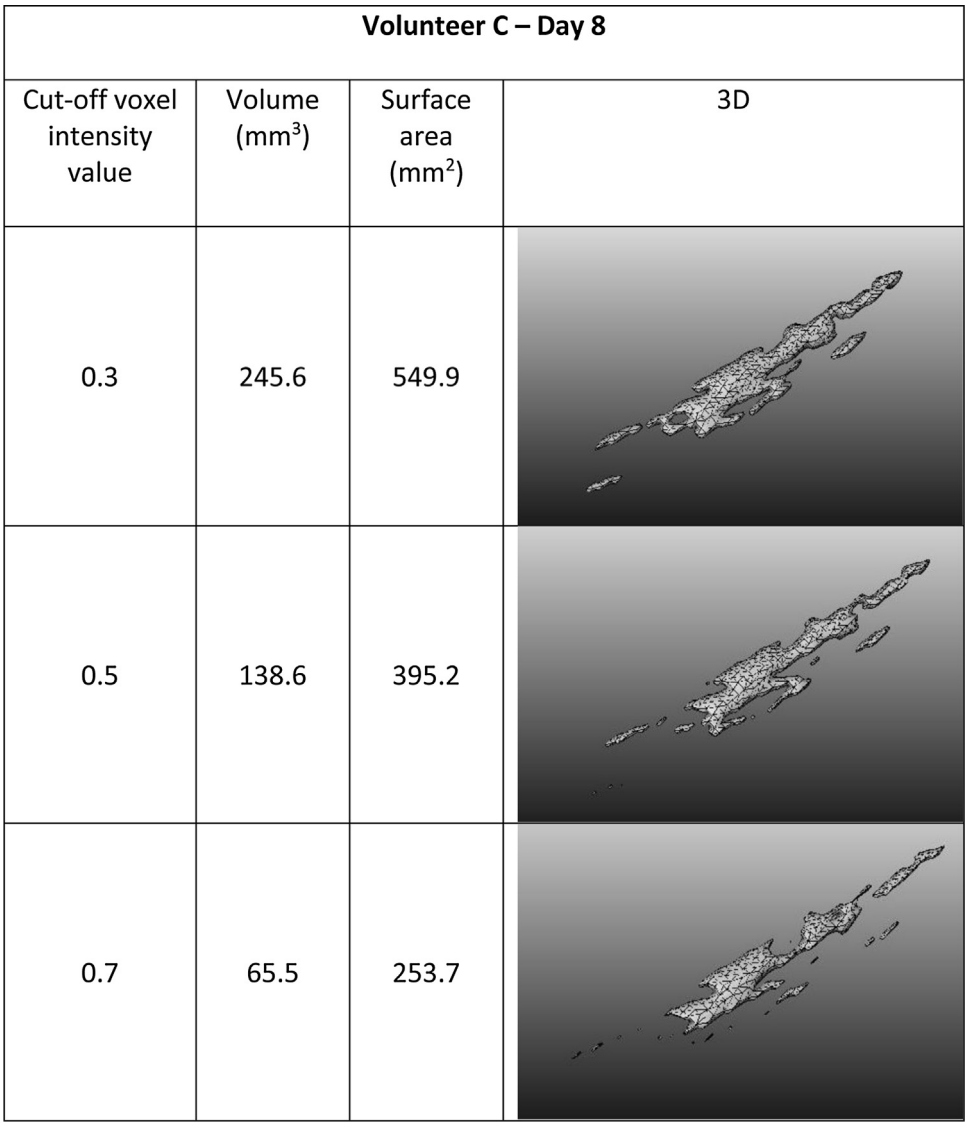

Fig. 9. Different depot properties using 0.3, 0.5 and 0.7 as cut-off voxel intensity value for fat fraction labelling. Data was obtained from volunteer C at day 8.

result in a fine dispersion of small oil droplets emulsified in interstitial fluid. These droplets are not anymore attached to the main part of the oil depot. It can be speculated that these small droplets are individually cleared from the injection site. Although there is no clearance or digestion mechanism published yet, it can be suggested that these droplets can be transported towards the lymphatics or stay attached to the muscle fibres (Fig. 6). As a result of this speculation, these small droplets have a relative high surface area that may cause a quicker oil depot depletion of compounds.

Furthermore, the voxel intensity value of 0.5 used in this study may result in a false positive result of the oil depot, because a voxel intensity value of <0.5 gives a lower oil depot volume. The variety in depot disappearance rates from the injection site is noticeable in Fig. 7. The residence time of the i.m. oil depots in our volunteers seems to be much shorter than in pigs, as reported by Larsen et al. (Larsen et al., 2001). In human, the depot could be visualised for 2–14 days after injection, whereas the half-life of 21.4 days in pigs was reported. Because of the accuracy studies with the fixed oil volumes, the voxel intensity value of 0.5 was considered as reliable. An obvious explanation for this difference in disappearance rate may be the contraction frequency of the injection site. It is assumed that the human upper arm muscle may have a higher frequency compared to neck muscle in pigs. As a result, this may increase drug release and subsequently absorption from oil depots. Although the drug absorption from oil depot injections during exercise is unknown, the drug absorption from aqueous injections (e.g. insulin injections) during exercise is increased (Berger et al., 1982; Frid et al., 1990; Koivisto and Felig, 1978; Titulaer et al., 1993).

4. Conclusion

The MRI method applied in this study is able to visualise the shape of an oil depot when injected in the muscle. The method enables to estimate the surface area as well as the way the oil is disappeared from the injection site. From this, further understanding can be obtained about the mechanism of drug absorption from oil depots. During the development of an i.m. injection, it should be taken into account that a stretched shape of the oil depot is formed in muscle. It can be argued that the oil depot is squeezed between the muscle fibres, which explains the obtained shape. As a result of this shape, the determined surface area is much larger than that of a perfect sphere that is used in mathematical models. Although the surface areas were approximately the same in all volunteers

directly after injection, this was not the case in the successive days. Furthermore, the oil depot disappearance from the injection site is very variable between patients after i.m. injection. In all cases, the oil depot was disappeared from the injection site within 14 days. These factors are relevant for the absorption kinetics of active substances from oil depots and therefore contribute to the optimal therapeutic treatment in patients.

Conflicts of interest

The authors declare no conflict of interest.

Acknowledgments

The authors would like to thank nurses Loes ten Brink and Albertine van der Veen-Selderbeek for their contribution to this research.

References

Bagchus, W.M., Smeets, J.M.W., Verheul, H.A.M., De Jager-Van Der Veen, S.M., Port, A., Geurts, T.B.P., 2005. Pharmacokinetic evaluation of three different intramuscular doses of nandrolone decanoate: analysis of serum and urine samples in healthy men. J. Clin. Endocrinol. Metab. 90, 2624–2630. doi:http://dx.doi.org/10.1210/jc.2004-1526.

Berger, M., Cuppers, H.J., Hegner, H., Jorgens, V., Berchtold, P., 1982. Absorption kinetics and biologic effects of subcutaneously injected insulin preparations. Diabetes Care 5, 77–91. doi:http://dx.doi.org/10.2337/diacare.5.2.77.

Covell, N.H., McEvoy, J.P., Schooler, N.R., Stroup, T.S., Jackson, C.T., Rojas, I.A., Essock, S.M., 2012. Effectiveness of switching from long-acting injectable fluphenazine or haloperidol decanoate to long-acting injectable risperidone microspheres. J. Clin. Psychiatry 73, 669–675. doi:http://dx.doi.org/10.4088/JCP.11m07074.

Düsterberg, B., Nishino, Y., 1982. Pharmacokinetic and pharmacological features of oestradiol valerate. Maturitas 4, 315–324.

Dixon, W.T., 1984. Simple proton spectroscopic imaging. Radiology 153, 189–194. doi:http://dx.doi.org/10.1148/radiology.153.1.6089263.

Edelstein, D., Basaria, S., 2010. Testosterone undecanoate in the treatment of male hypogonadism. Expert Opin. Pharmacother. 11, 2095–2106. doi:http://dx.doi.org/10.1517/14656566.2010.505920.

Frid, A., Ostman, J., Linde, B., Background, C., 1990. Hypoglycemia risk during exercise after intramuscular injection of insulin in thigh in IDDM. Diabetes Care 13, 473–477. doi:http://dx.doi.org/10.2337/diacare.13.5.473.

Geusens, P., 1995. Nandrolone decanoate: pharmacological properties and therapeutic use in osteoporosis. Clin. Rheumatol. 14, 32–39. doi:http://dx.doi.org/10.1007/BF02210686.

Hu, H.H., Kim, H.-W., Nayak, K.S., Goran, M.I., 2010. Comparison of fat–water MRI and single-voxel MRS in the assessment of hepatic and pancreatic fat fractions in humans. Obesity 18, 841–847. doi:http://dx.doi.org/10.1038/oby.2009.352.

Kalicharan, R.W., El Amrani, M., Schot, P., Vromans, H., 2016a. Pharmacokinetics in elderly women of benzyl alcohol from an oil depot. J. Pharm. Sci. 105, 1519–1525. doi:http://dx.doi.org/10.1016/j.xphs.2016.01.022.

Kalicharan, R.W., Schot, P., Vromans, H., 2016b. Fundamental understanding of drug absorption from a parenteral oil depot. Eur. J. Pharm. Sci. 83, 19–27. doi:http://dx.doi.org/10.1016/j.ejps.2015.12.011.

Koivisto, V.A., Felig, P., 1978. Effects of leg exercise on insulin absorption in diabetic patients. N. Engl. J. Med. 298, 79–83. doi:http://dx.doi.org/10.1056/NEJM197801122980205.

Kuijf, H.J., 2013. Image Processing Techniques for Quantification and Assessment of Brain MRI. Utrecht University, The Netherlands.

Larsen, S.W., Rinvar, E., Svendsen, O., Lykkesfeldt, J., Friis, G.J., Larsen, C., 2001. Determination of the disappearance rate of iodine-125 labelled oils from the injection site after intramuscular and subcutaneous administration to pigs. Int. J. Pharm. 230, 67–75. doi:http://dx.doi.org/10.1016/S0378-5173(01)00860-2.

Larsen, C., Larsen, S.W., Jensen, H., Yaghmur, A., Ostergaard, J., 2009. Role of in vitro release models in formulation development and quality control of parenteral depots. Expert Opin. Drug Deliv. 6, 1283–1295. doi:http://dx.doi.org/10.1517/17425240903307431.

Luo, J.P., Hubbard, J.W., Midha, K.K., 1997. Studies on the mechanism of absorption of depot neuroleptics: fluphenazine decanoate in sesame oil. Pharm. Res 14, 1079–1084.

Ma, J., 2008. Dixon techniques for water and fat imaging. J. Magn. Reson. Imaging 28, 543–558. doi:http://dx.doi.org/10.1002/jmri.21492.

Minto, C.F., Howe, C., Wishart, S., Conway a, J., Handelsman, D.J., 1997. Pharmacokinetics and pharmacodynamics of nandrolone esters in oil vehicle: effects of ester, injection site and injection volume. J. Pharmacol. Exp. Ther. 281, 93–102.

Morgentaler, A., Dobs, A.S., Kaufman, J.M., Miner, M.M., Shabsigh, R., Swerdloff, R.S., Wang, C., 2008. Long acting testosterone undecanoate therapy in men with hypogonadism: results of a pharmacokinetic clinical study. J. Urol. 180, 2307–2313. doi:http://dx.doi.org/10.1016/j.juro.2008.08.126.

Nelson, K.G., Shah, A.C., 1975. Convective diffusion model for a transport-controlled dissolution rate process. J. Pharm. Sci. 64, 610–614. doi:http://dx.doi.org/10.1002/jps.2600640407.

Novakovic, V., Adel, T., Peselow, E., Lindenmayer, J.-P., 2013. Long-acting injectable antipsychotics and the development of postinjection delirium/sedation syndrome (PDSS). Clin. Neuropharmacol. 36, 59–62. doi:http://dx.doi.org/10.1097/WNF.0b013e3182854f70.

Philips Medical Systems, 2008. Basic Principles of MR Imaging. Philips Medical Systems.

Prettyman, J., 2005. Subcutaneous or intramuscular? Confronting a parenteral administration dilemma. MEDSURG Nurs. 14, 93–99.

Querleux, B., Cornillon, C., Jolivet, O., Bittoun, J., 2002. Anatomy and physiology of subcutaneous adipose tissue by in vivo magnetic resonance imaging and spectroscopy: relationships with sex and presence of cellulite. Skin Res. Technol. 8, 118–124. doi:http://dx.doi.org/10.1034/j.1600-0846.2002.00331.x.

Ren, J., Dimitrov, I., Sherry, A.D., Malloy, C.R., 2008. Composition of adipose tissue and marrow fat in humans by 1H NMR at 7 Tesla. J. Lipid Res. 49, 2055–2062. doi:http://dx.doi.org/10.1194/jlr.D800010-JLR200.

Ritter, F., Boskamp, T., Homeyer, A., Laue, H., Schwier, M., Link, F., Peitgen, H., 2011. Medical image analysis. IEEE Pulse 2, 60–70. doi:http://dx.doi.org/10.1109/MPUL.2011.942929.

Shaik, I.H., Bastian, J.R., Zhao, Y., Caritis, S.N., Venkataramanan, R., 2015. Route of administration and formulation dependent pharmacokinetics of 17-hydroxyprogesterone caproate in rats. Xenobiotica 8254, 1–6. doi:http://dx.doi.org/10.3109/00498254.2015.1057547.

Soni, S.M., Wiles, D., Schiff, a. a., Bamrah, J.S., 1988. Plasma levels of fluphenazine decanoate: effects of site of injection, massage and muscle activity. Br. J. Psychiatry 153, 382–384. doi:http://dx.doi.org/10.1192/bjp.153.3.382.

Titulaer, H., a Eling, W.M., Zuidema, J., 1993. Pharmacokinetic and pharmacodynamic aspects of artelinic acid in rodents. J. Pharm. Pharmacol. 45, 830–835.

Uchida, T., Suzuki, T., Sakurai, H., Tsutsumi, C., Den, R., Mimura, M., Uchida, H., 2013. Ten year outcomes of outpatients with schizophrenia on conventional depot antipsychotics. Int. Clin. Psychopharmacol. 28, 261–266. doi:http://dx.doi.org/10.1097/YIC.0b013e328363aa5a.

Van Weringh, G., Komen, B.J., Thieme, R.E., van der Hoeven, R.T.M., Vos, T., 1994. Comparative bioavailability study of two haloperidol decanoate containing products. Pharm. World Sci. 16, 343–347. doi:http://dx.doi.org/10.1007/BF02178564.

Weng Larsen, S., Larsen, C., 2009. Critical factors influencing the in vivo performance of long-acting lipophilic solutions—impact on in vitro release method design. AAPS J. 11, 762–770. doi:http://dx.doi.org/10.1208/s12248-009-9153-9.

Wijnand, H.P., Bosch, A.M.G., Donker, C.W., 1985. Pharmacokinetic parameters of nandrolone (19-nortestosterone) after intramuscular administration of nandrolone decanoate (Deca-Durabolin(R)) to healthy volunteers. Eur. J. Endocrinol. 110, S19–S30. doi:http://dx.doi.org/10.1530/acta.0.109s00019.